JOURNAL OF GUIDANCE, CONTROL, AND DYNAMICS
Vol. 34, No. 2, March–April 2011

Engineering Notes

Analysis of Insect-Inspired Wingstroke Kinematic Perturbations for Longitudinal Control

J. Sean Humbert* and Imraan Faruque†
University of Maryland, College Park, Maryland 20742

DOI: 10.2514/1.51912

I. Introduction

INSECTS display remarkable agility and flight-path control in the execution of their everyday tasks, all in the face of significant environmental uncertainties. Maneuvering forces are typically generated by small kinematic perturbations to high-frequency wing motions, such as changes in stroke amplitude, timing of wing rotation, or stroke plane tilting [1]. This clever approach of coupling high-frequency actuation with low-frequency rigid-body motion eliminates the need in most species for active sensing on and active deformation of the wing surface, otherwise evident in their avian [2] and mammalian [3] aerobatic counterparts.

Previous analysis of insect-inspired flapping-wing locomotion has examined wing kinematic trajectories from the perspective of maximizing lift [4,5] or minimizing required power [6]. With the introduction of new tools to extract the fine wingstroke to wingstroke kinematics of insects from high-speed videography [7,8], a number of species-specific control strategies for maneuvering have been identified. In addition, with the development of microscale vehicles that can potentially generate lift forces greater than their weight [9], stability and control aspects of the problem are now a focal point of research.

Despite the critical need, the inherent complexity of small-scale flapping flight aerodynamics has obscured a control-theoretic analysis of both biologically relevant and engineered wing kinematic perturbation strategies. While the detailed aerodynamic mechanisms involved in small-scale flight are still an area of active research [10], recent efforts have in fact yielded several approaches for extraction of reduced-order linear time-invariant (LTI) flight dynamics, either for single-degree-of-freedom experimental cases [11,12], direct analytic methods [13], or more general computationally [14] and spectrally derived models [15]. Such formulations are amenable to application of linear control analysis tools, and they should provide the next level of insight.

Reachability (or more traditionally, controllability) characterizes the amount of control one has over the state of a system through the choice of the input. This is an important topic for small-scale flapping-wing micro air vehicle (MAV) designers for several reasons. Size, weight, and power (SWAP) constraints are very stringent at this scale, and reductions in complexity that promote robustness and weight reduction are encouraged. In addition, these vehicles are intended to operate in gusty and possibly cluttered environments, and a high level of platform maneuverability and actuation authority will be crucial to achieving robust flight-path control in the face of these uncertainties.

This Note explores the reachable state space associated with biologically inspired kinematic control strategies seen in longitudinal motion about hover. In Sec. II, a frequency-based system identification methodology for identifying the stability derivatives of a small-scale flapping microsystem about hover is outlined, along with the control derivatives for biologically relevant wing kinematic perturbations for maneuvering. Section III applies controllability analysis tools to interpret these biologically relevant control strategies for MAV design, using the example of an MAV with *Drosophila*-like parameters.

II. Longitudinal Flight Dynamics Modeling

The flight dynamics of small-scale flapping-wing insects are governed by unsteady aerodynamic mechanisms associated with leading-edge vortex growth and shedding, unsteady rotational forces, wing–wake interactions, and added mass effects [16]. Maneuvering forces are generated by small kinematic perturbations to high-frequency wing motions, such as differential stroke amplitudes or stroke plane tilting. When the resulting aerodynamics are coupled to rigid-body equations of motion, the result is a nonlinear time-dependent set of differential equations where the system state is the rigid-body/wing configuration and velocity, and the control inputs are the prescribed perturbations to wing kinematics.

The general form of the governing flight dynamics equations are clearly very complex, and several assumptions must be made in order to proceed with a controllability analysis. The first assumption is that of quasi-steady aerodynamics [17], based on experimental fits to a dynamically scaled robotic mechanism. While the original formulation of the quasi-steady model proposes lift and drag as purely functions of the instantaneous wing motion, the aerodynamic forces are also functions of the body motion throughout the surrounding fluid, and mechanisms to account for the dependence have been the subject of recent study [11,12,15], giving rise to passive aerodynamic damping.

The second simplifying assumption is that the instantaneous aerodynamic lift and drag on the rigid body are approximated by wingstroke-averaged forces to provide estimates of the vehicle stability and control derivatives. This application of averaging theory has been investigated previously and shown to be useful for reducing systems where high-frequency actuation is coupled to low-frequency rigid-body motions [18]. Under this assumption, the explicit time dependence is removed, which permits the formulation of LTI flight dynamics models of the form

$$\dot{x} = Ax + Bu \tag{1}$$

In this case, $A \in \mathbb{R}^{n\times n}$ and $B \in \mathbb{R}^{n\times p}$ represent the state and input matrices, $u(t) \in L_2^p[0,\infty)$ represents the input time history, and $x \in L_2^n[0,\infty)$ represents the state history of the model. These components form the basis for system identification of the full nonlinear system.

To facilitate the identification of the stability derivatives in A and the control derivatives in B for each of the inputs, the underlying flight mechanics are posed as rigid-body dynamics paired with quasi-steady aerodynamics, including the effects of state perturbations from the equilibrium to create a nonlinear simulation (Fig. 1). Recent work [15] has placed the quasi-steady aerodynamic formulation in the context of state perturbations from a reference condition via an

Received 13 August 2010; revision received 18 October 2010; accepted for publication 21 October 2010.

*Assistant Professor, Department of Aerospace Engineering, 3182 Glenn L. Martin Hall; humbert@umd.edu. Senior Member AIAA.

†Graduate Research Assistant, Department of Aerospace Engineering, 3182 Glenn L. Martin Hall; imraan@umd.edu.

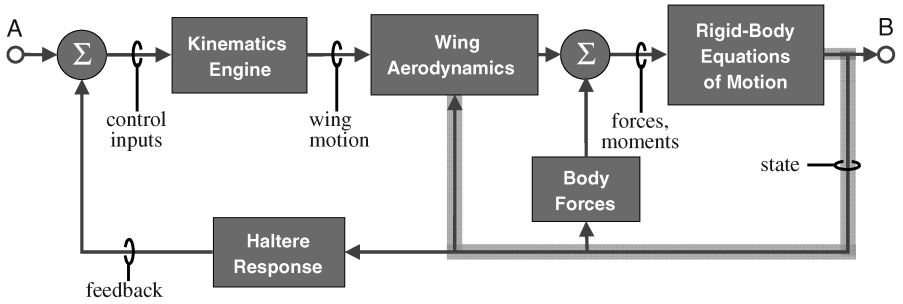

Fig. 1 Full nonlinear simulation used for system identification of *Drosophila melanogaster* flight dynamics, including state-dependent quasi-steady aerodynamics, rigid-body equations of motion, body drag, and haltere rate feedback.

updated definition of the wing tip speed and wing angle of attack. The current study uses the aerodynamic model detailed in Faruque and Humbert [15] to include the effects of rotational and translational rigid-body motions. The revised wing tip speed affects both the dynamic pressure and angle of attack, which accounts for passive aerodynamic damping [15,19,20]. In addition, *Dipteran* insects use mechanosensory halteres that have been shown to act as high-frequency biological rate gyros [21,22]. Previous work has characterized the haltere frequency responses in both equilibrium [23] and aggressive flight motions, known as saccades, showing that they can be modeled as bandpass filters [24,25]. In the simulation, simple bandpass filters with biologically based parameters on the angular rates are used in a feedback loop to model the haltere angular rate feedback.

The nominal (trim) kinematics [6,15] are assumed to be a periodic oscillation $\phi(t)$ contained in a stroke plane inclined at angle β from horizontal, with the wing intersecting the stroke plane at angle $\alpha_g(t)$. For longitudinal motions, the left and right wings are actuated together, and the control parameter is the same on both. Biologically relevant control inputs considered in this study (Fig. 2) were modeled after previous free-flight *Drosophila* studies, including 1) stroke plane inclination [1] β_c: a tilting of the stroke plane generating pitch moment and forward force, 2) stroke plane offset [1,26,27] ϕ_{off}: a fore/aft shift of the wing sweep used primarily to generate pitch moment, and 3) asymmetric wing angle [8] α_{ud}: an upstroke/downstroke asymmetry in the angle of the wing relative to the stroke plane, used primarily to generate forward force.

Frequency sweeps (chirp signals) were applied to three selected inputs to excite the longitudinal dynamics of the insect. Based on the spectral response of the input $G_{xx}(\omega)$ and output $G_{yy}(\omega)$ (calculated by the chirp z transform), the transfer function G was found via

$$G(\omega) = \frac{G_{yy}(\omega)}{G_{xx}(\omega)} \tag{2}$$

An example of the ϕ_{off}-to-θ input/output pair is shown in Fig. 3a. This frequency-based system identification approach is attractive over analytical linearization or computational fluid dynamics methods, since the frequency range over which the linear model accurately represents the full nonlinear dynamics can be determined by the coherence:

$$\gamma(\omega) = \frac{|G_{xy}(\omega)|^2}{G_{xx}(\omega)G_{yy}(\omega)} \tag{3}$$

The stability and control derivatives in the flight dynamics model (4) were selected to maximize coherence in the low-frequency regions (up to 20 Hz) while discarding the small periodic high-frequency motion. The coherence for the ϕ_{off}-to-θ input/output pair is shown in Fig. 3a. Note that, with the haltere feedback about the pitch axis, the longitudinal system is stable (Fig. 3b) and the matrix A is Hurwitz.

The general state-space model structure for the longitudinal dynamics with the control inputs listed previously is given by

$$\begin{bmatrix} \Delta\dot{u} \\ \Delta\dot{w} \\ \Delta\dot{q} \\ \Delta\dot{\theta} \end{bmatrix} = \begin{bmatrix} X_u & 0 & 0 & -g \\ 0 & Z_w & 0 & 0 \\ M_u & 0 & M_q & 0 \\ 0 & 0 & 1 & 0 \end{bmatrix} \begin{bmatrix} \Delta u \\ \Delta w \\ \Delta q \\ \Delta\theta \end{bmatrix} + \begin{bmatrix} 0 & X_\beta & X_{\phi_{\text{off}}} & X_{\alpha_{\text{ud}}} \\ Z_\Phi & 0 & 0 & 0 \\ 0 & M_\beta & M_{\phi_{\text{off}}} & M_{\alpha_{\text{ud}}} \\ 0 & 0 & 0 & 0 \end{bmatrix} \begin{bmatrix} \Phi_c \\ \beta_c \\ \phi_{\text{off}} \\ \alpha_{\text{ud}} \end{bmatrix} \tag{4}$$

The general state-space model includes an additional input, stroke amplitude Φ_c. Stroke amplitude affects only heave Δw dynamics and is decoupled from the other states and inputs. Accuracy of the stability and control derivatives in the identified model were estimated as part of the system identification procedure. Figure 3d provides uncertainty estimates for the parameters, where the standard deviations are derived from the Cramer–Rao bounds [28]. The qualitative properties of the eigenvalue map are preserved under this uncertainty, shown in Fig. 3b.

III. Reachability Analysis

For the longitudinal flight dynamics (4), the goal is to have a rigorous framework in which to quantify the effectiveness of the biologically relevant control strategies [1,8] that have been described in the previous section. As the heave Δw dynamics and the collective stroke amplitude control input Φ_c are decoupled from the remaining states in the linearized model, the pitch/fore/aft dynamics

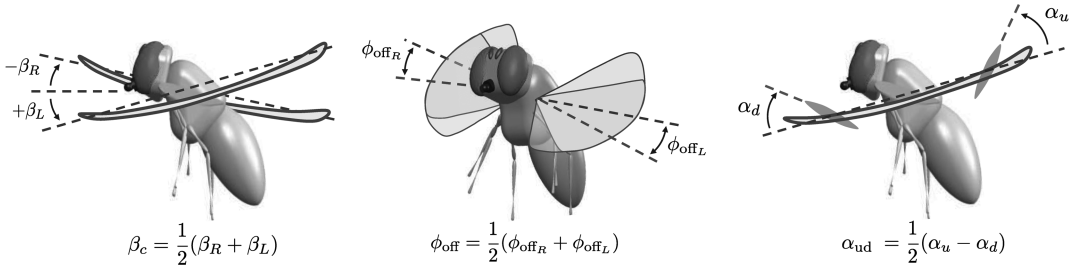

Fig. 2 Longitudinal control inputs: a) stroke plane inclination β_c, b) stroke plane offset ϕ_{off}, and c) differential wing angle α_{ud}.

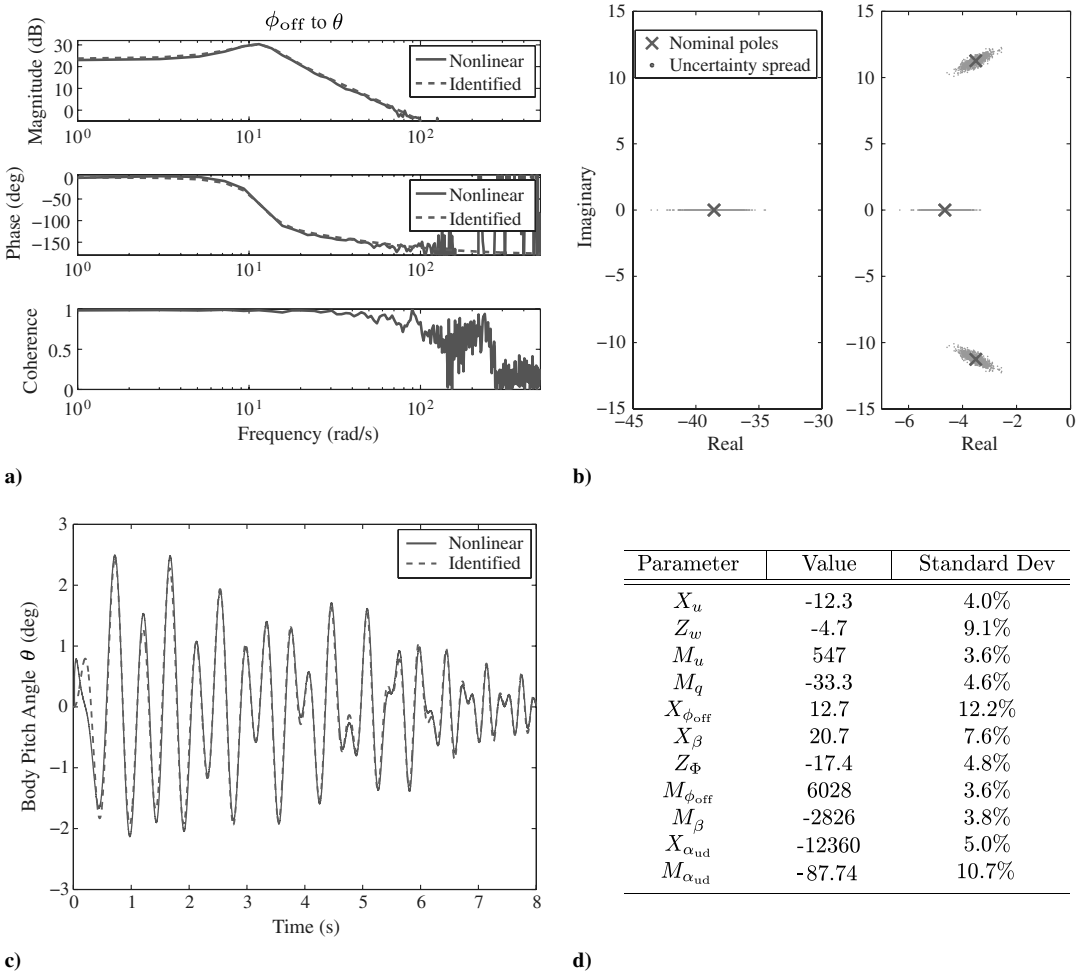

Parameter	Value	Standard Dev
X_u	-12.3	4.0%
Z_w	-4.7	9.1%
M_u	547	3.6%
M_q	-33.3	4.6%
$X_{\phi_{\text{off}}}$	12.7	12.2%
X_β	20.7	7.6%
Z_Φ	-17.4	4.8%
$M_{\phi_{\text{off}}}$	6028	3.6%
M_β	-2826	3.8%
$X_{\alpha_{\text{ud}}}$	-12360	5.0%
$M_{\alpha_{\text{ud}}}$	-87.74	10.7%

Fig. 3 Comparison of identified (reduced) and nonlinear models: a) transfer functions; b) pole structure, including uncertainty; c) time domain simulation; and d) uncertainty estimates for model parameters.

$(\Delta u, \Delta q, \Delta\theta)$ and control inputs $(\beta_c, \phi_{\text{off}}, \alpha_{\text{ud}})$ are considered without loss of generality.

Application of the controllability rank test for all possible combinations of control inputs reveals that the pitch/fore/aft system is fully controllable with any pair of the remaining control inputs, which motivates the examination of three input pairs:

$$u_1 = \begin{bmatrix} \beta_c \\ \phi_{\text{off}} \end{bmatrix}, \qquad u_2 = \begin{bmatrix} \beta_c \\ \alpha_{\text{ud}} \end{bmatrix}, \qquad u_3 = \begin{bmatrix} \phi_{\text{off}} \\ \alpha_{\text{ud}} \end{bmatrix} \tag{5}$$

To minimize actuator effort and maintain a small number of controls, we desire the pair of inputs that maximize the span of reachable states x_0 that result from any arbitrary input $u(t) \in L_2^p(-\infty, 0]$ of unit norm.

To quantify this, consider the controllability operator $x_0 = \Psi_c u$ for the LTI system (4):

$$\Psi_c \colon L_2^p(-\infty, 0] \to \mathbb{C}^n; \qquad u \to \int_{-\infty}^{0} e^{-A\tau} B u(\tau)\, \mathrm{d}\tau \tag{6}$$

As defined, Ψ_c maps the time history of the input $u(t)$ from $t = -\infty$ to a final state x_0 at $t = 0$. The set of reachable states for $\|u\| \le 1$ is then $\{\Psi_c u \colon u \in L_2^p(-\infty, 0], \|u\| \le 1\}$, which is equivalent to

$$\mathcal{E}_c = \{X_c^{1/2} x_c \colon x_c \in \mathbb{C}^n, \|x_c\| \le 1\} \tag{7}$$

$\mathcal{E}_c$ defines an ellipse in $\mathbb{C}^n$, for which the geometric properties are determined by the infinite-time controllability gramian X_c for the system (4)

$$X_c = \Psi_c \Psi_c^* = \int_0^\infty e^{A\tau} B B^* e^{A^*\tau}\, \mathrm{d}\tau \ge 0 \tag{8}$$

which can be computed given the matrix pair (A, B) via the Lyapunov equation

$$A X_c + X_c A^* + B B^* = 0 \tag{9}$$

The principle axes and lengths of $\mathcal{E}_c$ are given by the eigenvectors and eigenvalues of $X_c^{1/2}$, respectively, which motivates two control input ranking criteria. The first is the Frobenius norm of $X_c^{1/2}$:

$$\|X_c^{1/2}\|_F = \sqrt{\text{trace}[(X_c^{1/2}) \cdot X_c^{1/2}]} \tag{10}$$

for which the geometric interpretation is the square root of the summed squares of the axes lengths of $\mathcal{E}_c$. Second, since $X_c \ge 0$, one can also consider the volume $\det(X_c^{1/2})$ of $\mathcal{E}_c$ as a nonnegative measure of its size. Choosing control degrees of freedom that maximize either of these measures then corresponds to maximizing the set of reachable states over the choice of control degrees of freedom.

The controllability ellipsoids of the input pairs are shown in Figs. 4a–4c, indicating that the reachable space for a unit norm input increases significantly from input pair u_1 through u_3. For comparison, the reachable configuration space for a unit norm input on all three control terms $(\beta_c, \phi_{\text{off}}, \alpha_{\text{ud}})$ is shown as u_4 in Fig. 4d. The results of applying the two ranking criteria to the control input selections u_1 through u_4 are shown in Table 1 and plotted in Fig. 5. Out of the three pairs, clearly $u_3 = (\phi_{\text{off}}, \alpha_{\text{ud}})$ provides the most authority over the longitudinal dynamics. In terms of the reachable

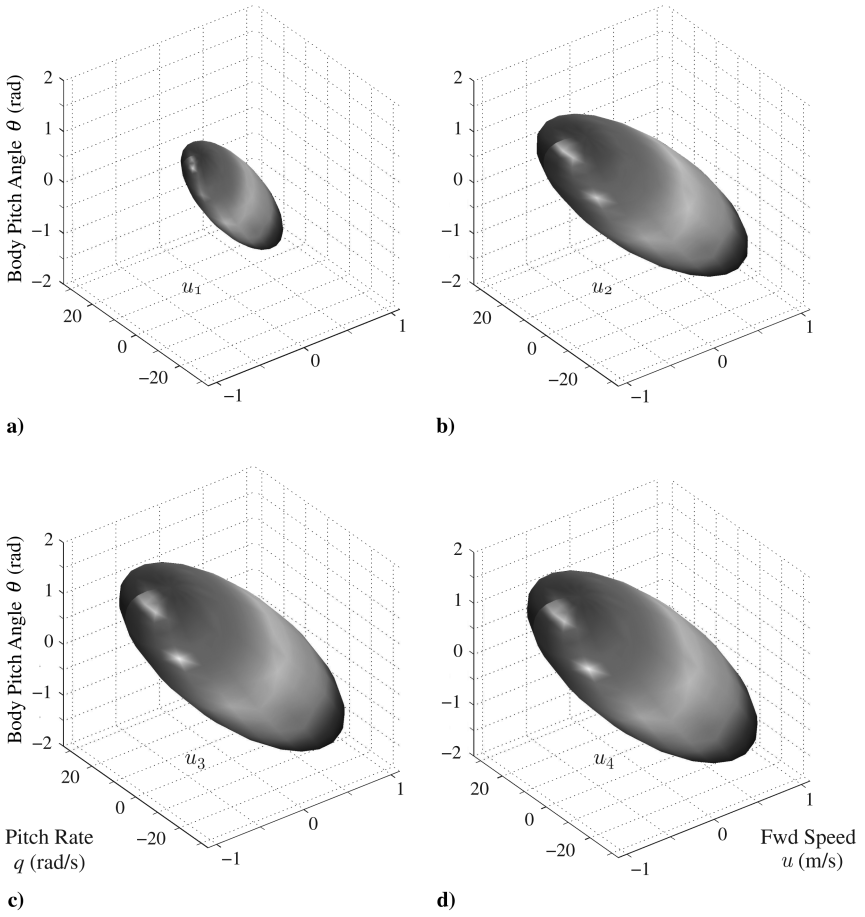

Fig. 4 Controllability ellipsoids for the input combinations illustrate the reachable configurations under the restriction $\|u_i\| \leq 1$. Input combinations u_1 through u_3 are pairs of control terms, while u_4 considers all three control terms ($\beta_c, \phi_{\text{off}}, \alpha_{\text{ud}}$).

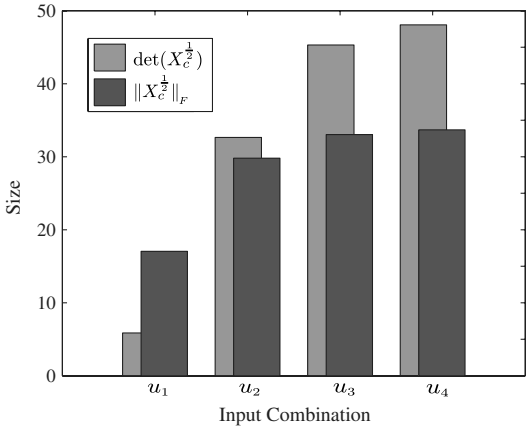

Fig. 5 Controllability of input combinations u_1 through u_4, as ranked by the determinant or Frobenius norm of the square root of the controllability gramian.

volume measure, u_3 provides a 672% increase over u_1 and a 38% increase over u_2. In addition, using all three control inputs u_4 only provides for a modest 6% increase in reachable volume over u_3. Similar conclusions follow from the Frobenius norm ranking criteria;

Table 1 Control input performance ranking criteria for u_1 though u_4

Input	u_1	u_2	u_3	u_4
$\det(X_c^{1/2})$	5.87	32.65	45.31	48.06
$\|X_c^{\frac{1}{2}}\|_F$	17.04	29.80	33.03	33.69

u_3 provides 94 and 11% increases over u_1 and u_2, respectively, whereas u_4 adds a 2% improvement over u_3.

The ellipsoidal interpretation also yields important information regarding the resulting system's controllability along particular directions in state space. In the case of Fig. 4, the rotational dominance of the control inputs (and modes) is evident in the larger reachable configuration space along the pitch rate/angle axes, while the range of forward speed is more limited.

IV. Conclusions

This Note introduces a control-theoretic framework and two performance measures for quantifying the state reachability for a given choice of biologically inspired wing kinematic control parameters, allowing for a set of candidate control strategies to be ranked. The work presented here leverages *Drosophila melanogaster* LTI flight dynamics models generated using a frequency-based system identification approach.

For the insect-size MAV example considered, all four of the input combinations provided full controllability, but the reachable space was dramatically improved through proper selection of the input combinations. The kinematic set that provided the most controllability involved a stroke bias term ϕ_{off} and an angle of attack difference in the upstroke and downstroke α_{ud}, which improved the reachable volume of state space 672% over the least controllable set. Moreover, while the reachable space was dramatically improved over each of the input pairs, only a slight advantage was found by combining all three inputs; adding a stroke plane angle degree of freedom β_c to the most effective pair resulted in only a modest increase (6%) in the volume of reachable state space.

The framework and performance measures introduced in this Note provide a means to appropriately choose kinematic inputs that minimize the required control energy and maximize the achievable

state space of the system. These tools can be applied to reduce actuator complexity to promote robustness and weight reduction, resulting in improved SWAP requirements for MAV flight stability and control. For MAV design, factors other than control energy (such as actuator geometry) may be the limitation on kinematic actuation, and a system-level approach must be used to determine the limiting factor. The framework introduced in this Note is directly applicable for a systems level model to be used in MAV design studies.

References

[1] Fry, S., Sayaman, R., and Dickinson, M., "The Aerodynamics of Free-Flight Maneuvers in *Drosophila*," *Science*, Vol. 300, No. 5618, 2003, pp. 495–498. doi:10.1126/science.1081944

[2] Carruthers, A., Thomas, A., and Taylor, G., "Automatic Aeroelastic Devices in the Wings of a Steppe Eagle *Aquila Nipalensis*," *Journal of Experimental Biology*, Vol. 210, No. 23, 2007, pp. 4136–4149. doi:10.1242/jeb.011197

[3] Swartz, S., Diaz, J., Riskin, D., Song, A., Tian, X., Willis, D., and Breuer, K., "Wing Structure and the Aerodynamic Basis of Flight in Bats," AIAA Aerospace Science Meeting, Reno, NV, AIAA Paper 2007-0042, 2007.

[4] Avadhanula, S., Wood, R. J., Steltz, E., Yan, J., and Fearing, R. S., "Lift Force Improvements for the Micromechanical Flying Insect," *IEEE/RSJ International Conference on Intelligent Robots and Systems*, Las Vegas, NV, IEEE Publ., Piscataway, NJ, 2003, pp. 1350–1356.

[5] Ansari, S. A., Knowles, K., and Zbikowski, R., "Insectlike Flapping Wings in the Hover Part 1: Effect of Wing Kinematics," *Journal of Aircraft*, Vol. 45, No. 6, 2008, pp. 1945–1954. doi:10.2514/1.35311

[6] Berman, G. J., and Wang, Z. J., "Energy-Minimizing Kinematics in Hovering Insect Flight," *Journal of Fluid Mechanics*, Vol. 582, 2007, pp. 153–168. doi:10.1017/S0022112007006209

[7] Fontaine, E., Zabala, F., Dickinson, M., and Burdick, J., "Wing and Body Motion During Flight Initiation in *Drosophila* Revealed by Automated Visual Tracking," *Journal of Experimental Biology*, Vol. 212, No. 9, 2009, pp. 1307–1323. doi:10.1242/jeb.025379

[8] Ristroph, L., Berman, G., Bergou, A., Wang, Z., and Cohen, I., "Automated Hull Reconstruction Motion Tracking (HRMT) applied to Sideways Maneuvers of Free-Flying Insects," *Journal of Experimental Biology*, Vol. 212, No. 9, 2009, pp. 1324–1335. doi:10.1242/jeb.025502

[9] Wood, R. J., "The First Takeoff of a Biologically Inspired At-Scale Robotic Insect," *IEEE Transactions on Robotics and Automation*, Vol. 24, No. 2, 2008, pp. 341–347. doi:10.1109/TRO.2008.916997

[10] Ramamurti, R., and Sandberg, W. C., "Computational Investigation of the Three-Dimensional Unsteady Aerodynamics of *Drosophila* Hovering and Maneuvering," *Journal of Experimental Biology*, Vol. 210, No. 5, 2007, pp. 881–896. doi:10.1242/jeb.02704

[11] Hesselberg, T., and Lehmann, F.-O., "Turning Behaviour Depends on Frictional Damping in the Fruit Fly *Drosophila*," *Journal of Experimental Biology*, Vol. 210, No. 24, 2007, pp. 4319–4334. doi:10.1242/jeb.010389

[12] Hesselberg, T., and Lehmann, F. O., "Corrigendum: Animal Flight Dynamics II. Longitudinal Stability in Flapping Flight," *Journal of Experimental Biology*, Vol. 210, 2007, pp. 4139–4334.

[13] Doman, D. B., Oppenheimer, M. W., and Sigthorsson, D. O., "Wingbeat Shape Modulation for Flapping-Wing Micro- Air-Vehicle Control During Hover," *Journal of Guidance, Control, and Dynamics*, Vol. 33, No. 3, 2010, pp. 724–739. doi:10.2514/1.47146

[14] Sun, M., Wang, J., and Xiong, Y., "Dynamic Flight Stability of Hovering Insects," *Acta Mechanica Sinica*, Vol. 23, No. 3, 2007, pp. 231–246. doi:10.1007/s10409-007-0068-3

[15] Faruque, I. A., and Humbert, J. S., "Dipteran Insect Flight Dynamics Part 1: Longitudinal Motion about Hover," *Journal of Theoretical Biology*, Vol. 264, No. 2, 2010, pp. 538–552. doi:10.1016/j.jtbi.2010.02.018

[16] Sane, S., "The Aerodynamics of Insect Flight," *Journal of Experimental Biology*, Vol. 206, No. 23, 2003, pp. 4191–4208. doi:10.1242/jeb.00663

[17] Sane, S. P., and Dickinson, M. H., "The Aerodynamic Effects of Wing Rotation and a Revised Quasi-Steady Model of Flapping Flight," *Journal of Experimental Biology*, Vol. 205, 2002, pp. 1087–1096.

[18] Deng, X., Schenato, L., and Sastry, S. S., "Flapping Flight for Biomimetic Robotic Insects: Part II, Flight Control Design," *IEEE Transactions on Robotics and Automation*, Vol. 22, No. 4, 2006, pp. 789–803. doi:10.1109/TRO.2006.875483

[19] Hedrick, T. L., Cheng, B., and Deng, X., "Wingbeat Time and the Scaling of Passive Rotational Damping in Flapping Flight," *Science*, Vol. 324, No. 5924, 2009, pp. 252–255. doi:10.1126/science.1168431

[20] Faruque, I. A., and Humbert, J. S., "Dipteran Insect Flight Dynamics Part 2: Lateral Motion about Hover," *Journal of Theoretical Biology*, Vol. 265, No. 3, 2010, pp. 306–313. doi:10.1016/j.jtbi.2010.05.003

[21] Nalbach, G., and Hengstenberg, R., "The Halteres of the Blowy Calliphora I: Kinematics and Dynamics," *Journal of Comparative Physiology*, Vol. 173, No. 3, 1993, pp. 293–300. doi:10.1007/BF00212693

[22] Taylor, G., and Krapp, H., "Sensory Systems and Flight Stability: What do Insects Measure and Why?," *Advances in Insect Physiology*, Vol. 34, No. 2, 2007, pp. 231–316. doi:10.1016/S0065-2806(07)34005-8

[23] Sherman, A., and Dickinson, M. H., "A Comparison of Visual and Haltere-Mediated Equilibrium Reflexes in the Fruit Fly *Drosophila Melanogaster*," *Journal of Experimental Biology*, Vol. 206, No. 2, 2003, pp. 295–302. doi:10.1242/jeb.00075

[24] Sherman, A., and Dickinson, M. H., "Summation of Visual and Mechanosensory Feedback in *Drosophila* Flight Control," *Journal of Experimental Biology*, Vol. 207, No. 1, 2004, pp. 133–142. doi:10.1242/jeb.00731

[25] Bender, J. A., and Dickinson, M. H., "Visual Stimulation of Saccades in Magnetically Tethered *Drosophila*," *Journal of Experimental Biology*, Vol. 209, No. 16, 2006, pp. 3170–3182. doi:10.1242/jeb.02369

[26] Oppenheimer, M. W., Doman, D. B., and Sigthorsson, D. O., "Dynamics and Control of a Biomimetic Vehicle Using Biased Wingbeat Forcing Functions: Part I, Aerodynamic Model," 48th AIAA Aerospace Sciences Meeting, AIAA Paper 2010-1023, Jan. 2010.

[27] Doman, D. B., Oppenheimer, M. W., and Sigthorsson, D. O., "Dynamics and Control of a Biomimetic Vehicle Using Biased Wingbeat Forcing Functions: Part II, Controller," 48th AIAA Aerospace Sciences Meeting, AIAA Paper 2010-1024, Jan. 2010.

[28] Tischler, M. B., and Cauman, M. G., "Comprehensive Identification from Frequency Responses," Vol. 3, U.S. Army Aviation and Troop Command TR 94-A-018, Sept. 1999.